

Multifunctional AIEgens: Ready Synthesis, Tunable Emission, Mechanochromism, Mitochondrial, and Bacterial Imaging

Meijuan Jiang, Xinggui Gu, Ryan T. K. Kwok, Ying Li, Herman H. Y. Sung, Xiaoyan Zheng, Yilin Zhang, Jacky W. Y. Lam, Ian D. Williams, Xuhui Huang, Kam Sing Wong, and Ben Zhong Tang*

Luminogens with aggregation-induced emission characteristics (AIEgens) are intriguing due to its rapid expansion in various high-tech applications. However, there is still in high demand on the development of novel AIEgens with easy preparation and functionalization, stable structures, tunable emissions, and high quantum efficiency. In this contribution, three AIEgens based on diphenyl isoquinolinium (IQ) derivatives are reported. They can be facilely synthesized and possess high structural stability, favorable visible light excitation, large Stokes shifts, high quantum yields, tunable colors, and sufficient two-photon absorption of near-infrared light. Importantly, they exhibit multifunctionalities. They exhibit mechanochromic property, making them capable to be applied for rewritable papers. They can also be applied in mitochondrial imaging with high specificity, cell permeability, brightness, biocompatibility, and photostability. They are promising for the applications in evaluation of mitochondrial membrane potential and image-guided cancer cell ablation. Last, they are able to stain bacteria in a wash-free manner. All these intriguing results suggest such readily accessible and multifunctional diphenyl IQ-based AIEgens provide a new platform for construction of advanced materials for practical applications.

1. Introduction


Energy, environment, and health are three main global challenges. Luminescent materials have paved the way in related

scientific discoveries and technological innovations owing to their high-energy converting efficiency, excellent sensitivity, in situ workability, noninvasiveness, and high spatial–temporal resolution.^[1] For examples, organic light-emitting diodes have largely saved the electric energy for illumination, fluorescent chemosensors have been used to detect the environmental pollutants, and fluorescent bio-probes enable scientists to see the fine structures and monitor biological processes that have never seen before in living systems. Practically, fluorescent materials are preferred to be used in solid state or aqueous solutions with the considerations of convenience and safety. But a thorny problem of aggregation-caused quenching (ACQ) for many conventional fluorescent dyes is raised. Their emissions are often partially or completely quenched in aggregated state as compared to their dilute solutions. Such ACQ effect greatly limits

their practical applications. Opposite to ACQ, a recently coined “aggregation-induced emission (AIE)” phenomenon has offered a solution to the ACQ problems and drawn great research attentions in science. With rotor–stator structures, AIE luminogens

Dr. M. Jiang, Prof. X. Gu, Dr. R. T. K. Kwok, Dr. Y. Li, Dr. H. H. Y. Sung, Dr. X. Zheng, Dr. J. W. Y. Lam, Prof. I. D. Williams, Prof. X. Huang, Prof. B. Z. Tang
Department of Chemistry
Hong Kong Branch of Chinese National Engineering Research Center for Tissue Restoration and Reconstruction Institute for Advanced Study
Division of Biomedical Engineering
State Key Laboratory of Molecular Neuroscience and Institute of Molecular Functional Materials
The Hong Kong University of Science and Technology
Clear Water Bay, Kowloon, Hong Kong, China
E-mail: tangbenz@ust.hk
Prof. X. Gu
Beijing Advanced Innovation Center for Soft Matter Science and Engineering (BAICAS)
Beijing University of Chemical Technology
Beijing 100029, China

Dr. Y. Zhang, Prof. K. S. Wong
Department of Physics
The Hong Kong University of Science and Technology
Clear Water Bay, Kowloon, Hong Kong, China
Prof. B. Z. Tang
Guangdong Provincial Key Laboratory of Brain Science Disease and Drug Development
HKUST Shenzhen Research Institute
No. 9 Yuexing First RD, South Area, Hi-Tech Park, Nanshan Shenzhen 518057, China
Prof. B. Z. Tang
Guangdong Innovative Research Team
SCUT-HKUST Joint Research Laboratory
State Key Laboratory of Luminescent Materials and Devices
South China University of Technology
Guangzhou 510640, China

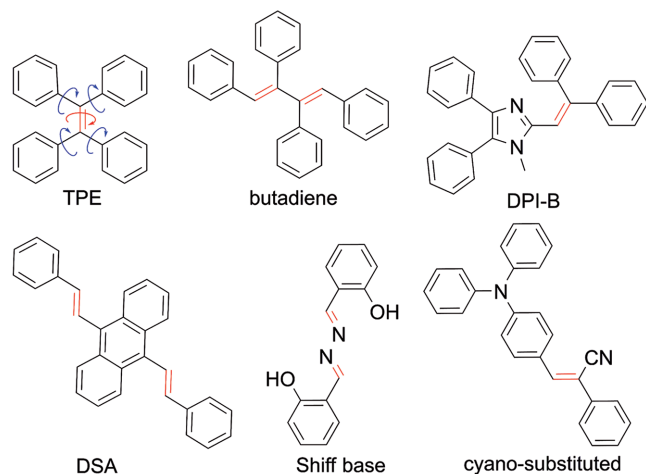
 The ORCID identification number(s) for the author(s) of this article can be found under <https://doi.org/10.1002/adfm.201704589>.

DOI: 10.1002/adfm.201704589

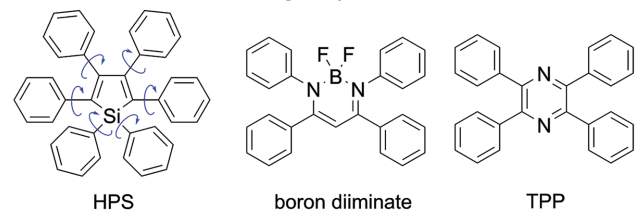
(AIEgens) are weakly emissive in solutions due to the ultrafast motions of the rotors consuming the exciton energy of excited molecules. They are highly emissive in the solid and aggregated states, where the intramolecular motions are mechanically restricted by the constraints of neighboring molecules and deleterious π - π stackings are eliminated due to the 3D conformations.^[2] The restriction of intramolecular motions (RIMs) is one of the most recognized mechanisms for the AIE phenomenon and AIE researches have grown exponentially since 2011.^[2a,3] It is envisioned that AIE materials hold great potential for solving the critical issues with the merits of high solid-state quantum yield, large Stokes shift, good photostability, and featured "turn-on" sensing. However, it fundamentally calls for new AIEgens with easy synthesis and functionalization to enable the AIE materials with the above fancy features.

So far, AIEgens with various core structures and functional groups have been developed (Scheme 1). Generally, the core structures of these molecular rotor-based AIEgens can be divided into two types. AIEgens in Type I are consisted of both aromatic rings and double bonds (C=C, C=N, N=N, etc.), such as tetraphenylethene (TPE),^[4] distyrylanthracene,^[5] imidazole-based analogues,^[6] butadienes,^[7] Schiff bases,^[8] and cyano-substituted derivatives.^[9] While in Type II, they are only consisted of aromatic rings, such as hexaphenylsilole (HPS),^[3a,10] borondiiminates,^[11] and tetraphenylpyrazine (TPP).^[12] The Type I AIEgens are relatively easy to synthesize and functionalize, so that a rich variety of AIEgens have been developed and used for practical applications. However, they suffer from defects of the double bonds: (1) *E/Z* isomers with different properties in photophysics and sensing are formed during syntheses. The isomers are very hard

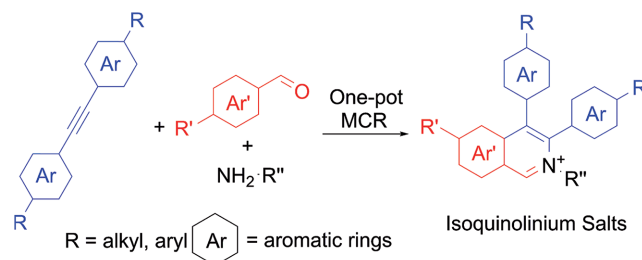
Type I Rotatable aromatic rings+double bonds



Type II Rotatable aromatic rings only



Scheme 1. Chemical structures of typical AIEgens.

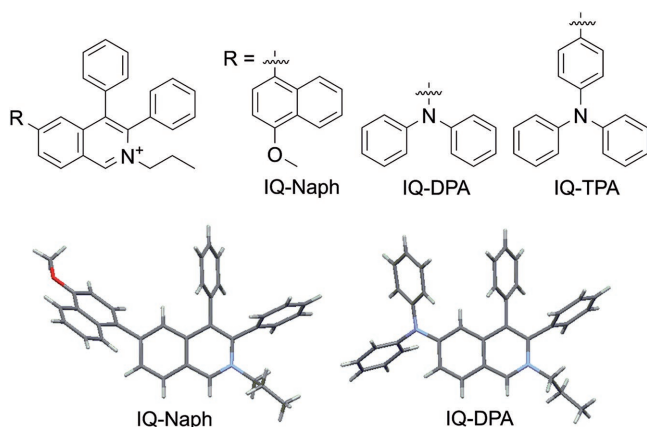


Scheme 2. One-pot multicomponent reaction of isoquinolinium salts.

to separate and thus they are often used in a mixture, leading to a complicated situation of mechanistic understanding;^[13] (2) many double-bond containing AIEgens, such as Schiff bases and dicyano-substituted compounds, are vulnerable to nucleophiles, such as CN^- , HS^- , and OH^- ,^[14] making them chemically unstable; and (3) the double bonds easily undergo photoisomerization and photooxidation upon excitation, leading to low photostability.^[12] On the other hand, Type II AIEgens are of well-defined structures with more clear AIE mechanism, better chemical and photostabilities. Their syntheses, however, are not readily accessible, and they require multiple steps and strict synthetic conditions.^[12] Thus, it would be satisfactory to integrate the merits of Types I and II and to develop novel AIEgens.

With regard to find an easy synthetic method for new Type II AIEgens, we have noticed a one-pot multicomponent reaction of alkyne, aldehyde, and amine in previous reports (Scheme 2).^[15] Compared to previous synthetic methods of TPE and HPS, this one-pot multicomponent reaction exhibits plenty of advantages: (1) it is a simple reaction; (2) products can be easily purified due to the large polarity difference from reactants; (3) the reaction is efficient with high yield up to 93%; (4) the diphenyl isoquinolinium (IQ)-based products are probably AIE-active due to their highly twisted molecular structures according to RIM mechanism; (5) the in situ generated positive charge is a strong electron acceptor and it will be easy to tune the emission colors by changing electron donor; and (6) a huge pool of reactants and a large structural scope of products are available to serve for various applications. Therefore, this reaction is anticipated to be an excellent choice for construction of readily accessible Type II AIEgens.

In this contribution, three AIEgens of Type II, namely IQ-naphthalene (Naph), IQ-diphenylamine (DPA), and IQ-triphenylamine (TPA), have been prepared (Scheme 3). Aromatic donor groups of methoxyl Naph, DPA, and TPA were intentionally chosen to achieve fluorescent materials with longer excitation and emission wavelengths, which are of great interests in practical applications, especially for cell imaging. All of these compounds are AIE-active with visible light excitation, large Stokes shift, high quantum yield, sufficient two-photon excitation, and mechanochromic properties. More importantly, they exhibit multifunctionalities. They were found to be applicable in rewritable paper with large contrast, mitochondrial imaging with high specificity, biocompatibility and excellent photostability, and wash-free bacterial imaging. Interestingly, their cellular uptake was found dependent on mitochondrial membrane potential (MMP) and thus they can be potentially used for differentiating cancer cells and normal cells. All the results demonstrate that



Scheme 3. Molecular structures of IQ-Naph, IQ-DPA, and IQ-TPA and single crystal structures of IQ-Naph and IQ-DPA. The crystal structures of IQ-Naph and IQ-DPA were obtained and shown in the ellipsoid style. Hydrogen, carbon, nitrogen, and oxygen were shown in white, gray, blue, and red, respectively. The molecular disorder, counteranion, and solvent molecules are omitted for clarity.

the readily accessible diphenyl isoquinolinium derivatives can serve as a new platform for construction of multifunctional AIE-gens with easy synthesis and functionalization, which is encouraging for the development of novel luminescent materials for scientific discoveries and technological innovations.

2. Results and Discussion

2.1. Synthesis and Characterization

IQ-Naph, IQ-DPA, and IQ-TPA (Scheme 1) were synthesized via a one-pot reaction of corresponding aldehydes, diphenyl acetylene, and propylamine under the catalysis of $[\text{RhCp}^*\text{Cl}_2]_2$ with high yield of 60–85%. Their structures were confirmed with nuclear magnetic resonance (NMR) spectra and high resolution mass spectra (HR-MS) with satisfactory results (Figures S1–S9, Supporting Information). Single crystals of IQ-Naph and IQ-DPA were obtained and analyzed by single crystal X-ray diffraction (Scheme 1 and Figure S10, Supporting Information). It is noteworthy that the single crystal of IQ-DPA was only obtained after anion exchange from BF_4^- to PF_6^- . However, we failed to obtain the single crystal of IQ-TPA even after anion exchange. To keep consistent, the counteranion for all the compounds used for the rest experiments was BF_4^- without further notice. These compounds excluding unstable vinyl groups are expected to be more thermally stable. Thermal gravity analysis results show that the temperature for 5% weight loss is measured to be 305–324 °C (Figure S11, Supporting Information), which is 100 °C higher than

that of TPE. Such good thermal stability is an advantage for many applications, especially in optoelectronic devices.

2.2. Photophysical Properties

Since the positive charged IQ is a strong electron-withdrawing group, attachment of aromatic electron donor groups (Naph, DPA, and TPA) not only extends the π -conjugation but also forms a donor– π –acceptor (D– π –A) structure, thus shifting the wavelengths of absorption and emission to the visible range. As shown in Figure 1A and Table 1, the absorption maxima of IQ-Naph, IQ-DPA, and IQ-TPA in dimethylsulfoxide (DMSO) solutions are found at 395, 406, and 450 nm, respectively. The bathochromic shifts of these compounds should be ascribed to the increasing electron donating ability of the groups: Naph < DPA < TPA. Similarly, the absorption maxima of these compounds in the solid states show slight redshifts of <7 nm (Figure S12, Supporting Information and Table 1). In the same trend, the emission peaks in solid state located at 469, 520, and 563 nm (Figure 1B). While in the DMSO (Table 1 and Figure S13, Supporting Information), their emissions were redshifted compared to their solid states, which should be explained by the high polarity of DMSO and the twisted intramolecular charge transfer (TICT) effect of these D– π –A molecules. Besides the visible light excitation and emission, all of them possess large Stokes shifts of 129–213 nm in DMSO solutions, which are highly desirable for cell imaging applications to avoid UV damage to biosamples, reduce autofluorescence, and eliminate the inner filtering effect.

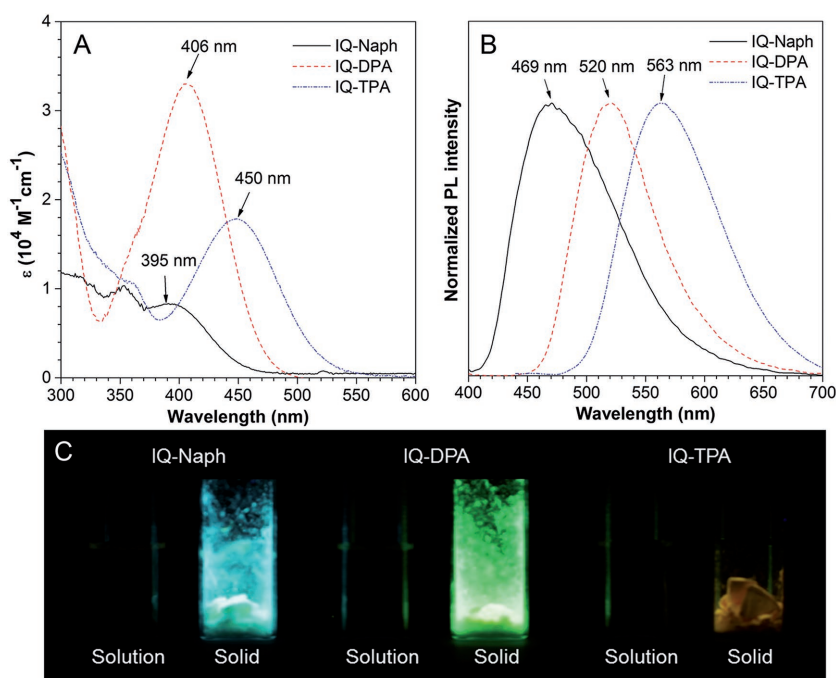


Figure 1. UV-vis absorption and photoluminescence spectra of IQ-Naph, IQ-DPA, and IQ-TPA. A) UV-vis absorption spectra of IQ-Naph, IQ-DPA, and IQ-TPA in DMSO solutions. Dye concentration = 10×10^{-6} M. B) PL spectra of IQ-Naph, IQ-DPA, and IQ-TPA in solid states. Excitation: 380 nm for IQ-Naph and IQ-DPA and 420 nm for IQ-TPA. C) Fluorescent photos of IQ-Naph, IQ-DPA, and IQ-TPA in DMSO solutions and solid states less than 365 nm UV irradiation.

Table 1. Photophysical properties of IQ-Naph, IQ-DPA, and IQ-TPA.

AIEgen	Solution ^{a)}			Solid state			Two-photon absorption		
	λ_{abs} [nm]	λ_{em} [nm]	$\Phi_{\text{F, soln.}}^{\text{b)}$	$\lambda_{\text{abs}}^{\text{c)}$ [nm]	$\lambda_{\text{em}}^{\text{d)}$ [nm]	$\Phi_{\text{F, solid}}^{\text{b,d)}$	$\alpha_{\text{AIE}}^{\text{e)}$	$\lambda_{2\text{PA}}^{\text{f)}$ [nm]	$\delta_{2\text{PA}}^{\text{f)}$ [GM]
IQ-Naph	395	596	0.023	402	469	0.53	23	820	76
IQ-DPA	406	535	0.001	410	520	0.57	570	840	107
IQ-TPA	450	663	0.011	455	563	0.19	17	900	215

^{a)} Measured in DMSO solutions; ^{b)} Determined using an integral sphere; ^{c)} Thin film made by spin-coating on quartz slide; ^{d)} Powders; ^{e)} α_{AIE} was defined as $\Phi_{\text{F, solid}}/\Phi_{\text{F, soln.}}$; ^{f)} Measured by a relative two-photon excited fluorescence technique and the details were described in the Supporting Information. 1 GM $\equiv 10^{-50}$ cm⁴ s per photon.

Structurally, the multiple rotatable aromatic (phenyl/naphthalene) rings may endow these compounds with AIE characteristics as their fast rotations could serve as nonradiative pathways to deactivate the excited states in the solutions and such rotational motions could be restricted in the aggregate state. As shown in Figure 1C and Table 1, these compounds are weakly emissive in DMSO solutions with quantum yield $\Phi_{\text{F, soln.}}$ of 0.001–0.023 and highly emissive in the solid powders with $\Phi_{\text{F, solid}}$ of 0.19–0.57. Their α_{AIE} ($\Phi_{\text{F, solid}}/\Phi_{\text{F, soln.}}$) values were calculated to be 17–570, suggesting a typical AIE feature of these compounds. For a comprehensive investigation, photoluminescence (PL) spectra of IQ-TPA were measured in DMSO/water mixtures with different water contents (Figure S14, Supporting Information). As the water fraction increased from 0 to 80 vol%, IQ-TPA is in molecular dissolving state and exhibits weak emission. However, further addition of water to 98 vol%, where a threshold of solubility was reached, IQ-TPA aggregates were formed and the fluorescence intensities at 627 nm were boosted with an 18-fold enhancement due to the RIM, demonstrating AIE characteristics. It is noted that the PL peaks of IQ-TPA were different in DMSO (663 nm), in DMSO-water mixtures of 98 vol% water fraction (627 nm), and in solid state (563 nm). Such a phenomenon is often seen in AIE compounds with strong D- π -A structures.^[4c,16] In the highly polar solvent DMSO, the emission of IQ-TPA is redshifted a lot from its solid states (563 nm) due to the strong TICT effect. While in DMSO-water mixtures of 98 vol% water fraction, the formation of aggregates increases the hydrophobicity of the local environment and excludes the polar solvent molecules, so the emission was blueshifted. As these AIE compounds show morphology-dependent emission which will be discussed in the mechanochromism part,^[17] the redshifted emission of the forming aggregates suggests their poor crystallinity (or amorphous state) where the molecules were loosely packed and may adopt a more planar conformation, thus showing a redder emission.

What's more, their nonlinear optical properties were studied. Their two-photon absorption maxima for IQ-Naph, IQ-DPA, and IQ-TPA are determined to be around 820, 860, and 900 nm, respectively, and their two-photon absorption cross sections are 76, 107, and 215 GM, respectively (Table 1 and Figure S15, Supporting Information). As small molecules, these values are quite large, thus providing them great potential as fluorescent probes for two-photon imaging.^[18]

2.3. Theoretical Calculations and Crystal Structures

To better understand the optical behaviors of these diphenyl isoquinolinium-based AIEgens, density functional theory

calculations were performed at the basis set of B3LYP/6-31G* via Gaussian 09. **Figure 2** shows the optimized structures and the frontier molecular orbitals of the AIEgens. The electron clouds of the highest occupied molecular orbitals (HOMOs) are mainly delocalized over the donor part of the molecules, while the electron clouds of the lowest unoccupied molecular orbitals (LUMOs) are localized on the isoquinolinium (acceptor) part. Their transition dipole moments from HOMO to LUMO were calculated to be 6.16 D for IQ-Naph, 4.73 D for IQ-DPA, and 10.12 D for IQ-TPA (Figure S16, Supporting Information). The substantial shifting of electron clouds indicates the occurrence of twisted intramolecular charge transfer in these AIEgens upon excitation, which is responsible for their large Stokes shifts and redshift in DMSO. Closely examining the optimized structures, we found that all the molecules adopt nonplanar 3D conformations: the phenyl groups on isoquinolinium core are highly twisted out from isoquinolinium plane with large dihedral angles of 74.4°–86.6° and aromatic groups of Naph, DPA, and TPA are also twisted with large angles of 24.4°–60.3°. These twisted aromatic rotating units would serve as rotors to quench the fluorescence nonradiatively in the solution state and prevent the molecules from detrimental π - π stacking in the crystals.

To support our explanation from theoretical calculations above, we carefully examined the obtained single crystal structures of IQ-Naph and IQ-DPA. Indeed, large torsional angles for the aromatic rotors were observed and the distances between the nearest two isoquinolinium planes are measured to be 7.84 Å for IQ-Naph and 5.55 Å for IQ-DPA, demonstrating there is no detrimental π - π interactions in the crystals (Figure S17, Supporting Information). The smaller torsional angles (63.9–72.4°) of the phenyl groups compared to that of the optimized structures (75.1–86.6°) should be attributed to the strong force field in the crystals posed by the multiple intermolecular interactions compared to the free force field of the vacuum. As shown in **Figure 3**, using IQ-Naph as an example, multiple weak intermolecular interactions, such as C-H...C, are found in the close-packed crystals and thought to be responsible for the RIMs. The weak intermolecular interactions of IQ-DPA are also highlighted in Figure S18 (Supporting Information). Above all, the AIE feature of these compounds can be attributed to the stator-rotor structures, twisted 3D conformations and multiple intermolecular interactions without detrimental π - π stackings.

2.4. Mechanochromism

From the structural view, AIEgens have stator-rotor structures with a highly twisted 3D conformations and the resulting

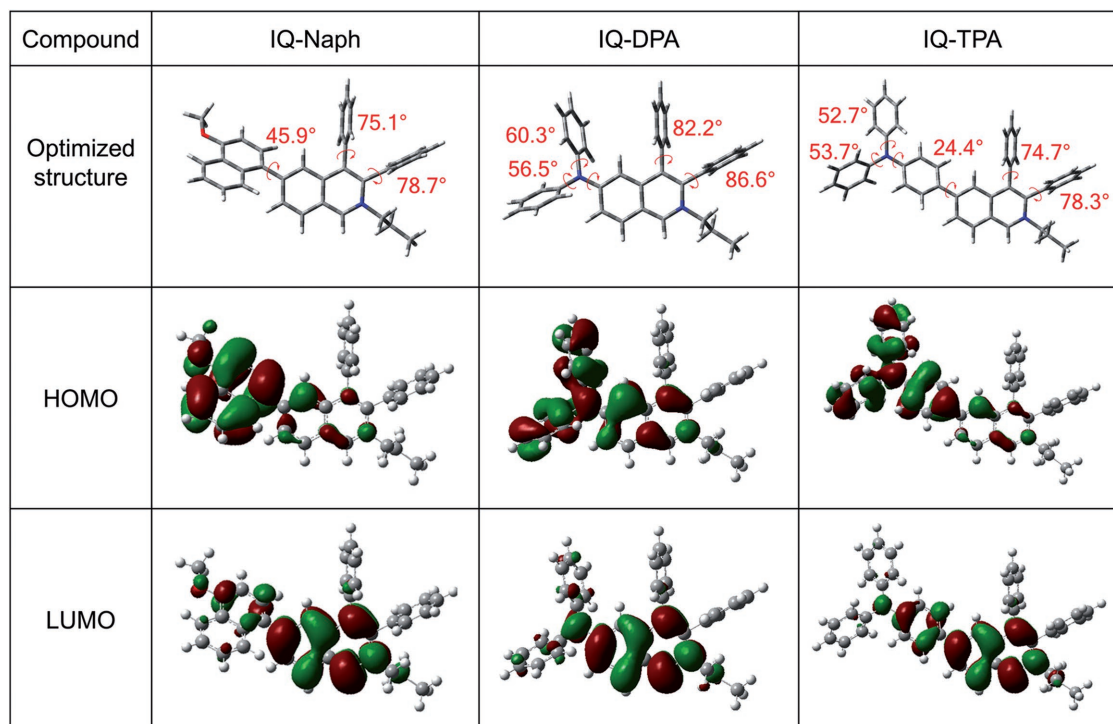


Figure 2. Optimized structures and frontier molecular orbitals for IQ-Naph, IQ-DPA, and IQ-TPA. Calculations were performed by density functional theory calculations at the B3LYP/6-31G* level using the Gaussian 09 program. Hydrogen, carbon, nitrogen, and oxygen were shown in white, gray, blue, and red, respectively. The dihedral angles from isoquinolinium plane of each phenyl groups were noted nearby.

loosely packed crystals are quite sensitive to external perturbation of mechanical force, thus leading to a chromic response. This phenomenon is termed as mechanochromism. Fluorescent materials with mechanochromic property are highly desirable in the applications of sensors, memory chips, optical storage, security inks, optoelectronic devices, and so forth.^[17,19] Therefore, we attempt to investigate the mechanochromism of the new AIEgens IQ-Naph, IQ-DPA, and IQ-TPA.

When the as-prepared powders were ground with a pestle on a glass slide, their apparent colors and fluorescent emissions were gradually redshifted and weakened with a large color contrast (Figure S19, Supporting Information and Figure 4A). PL

measurements show that the original emission maxima of IQ-Naph (469 nm), IQ-DPA (520 nm), and IQ-TPA (563 nm) were largely redshifted to the wavelengths of 547, 559, and 623 nm, respectively, after grinding (Figure S20, Supporting Information). Then, the powder samples before and after grinding were subjected to X-ray diffraction analysis and the results revealed that the as-prepared compounds were in polycrystalline state, while the grinded samples were in amorphous state (Figure 4B and Figure S21, Supporting Information), exhibiting a typical phenomenon of morphology-dependent emission.^[16,20] In the crystalline state, these molecules are orderly and closely packed, and the molecular conformations

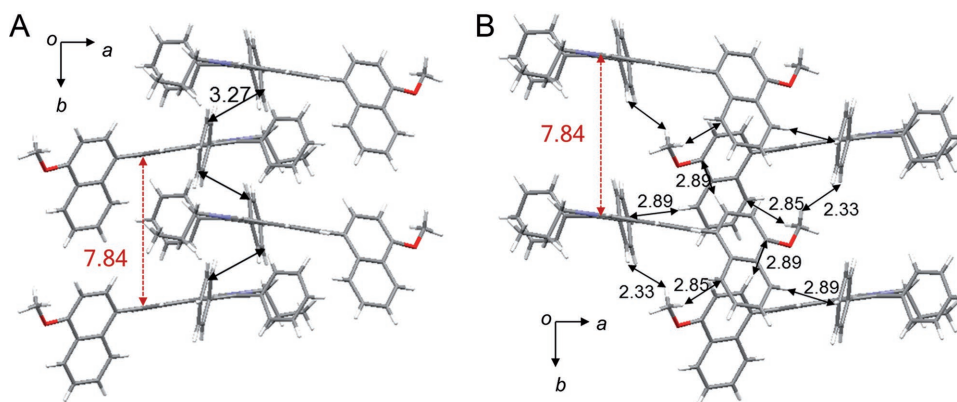


Figure 3. Crystal packing of IQ-Naph. A and B) The intermolecular distance between the neighboring isoquinolinium planes was noted. Intermolecular short contacts of IQ-Naph within sum of van der Waals radii were noted (unit: Å). Hydrogen, carbon, nitrogen, and oxygen were shown in white, gray, blue, and red, respectively.

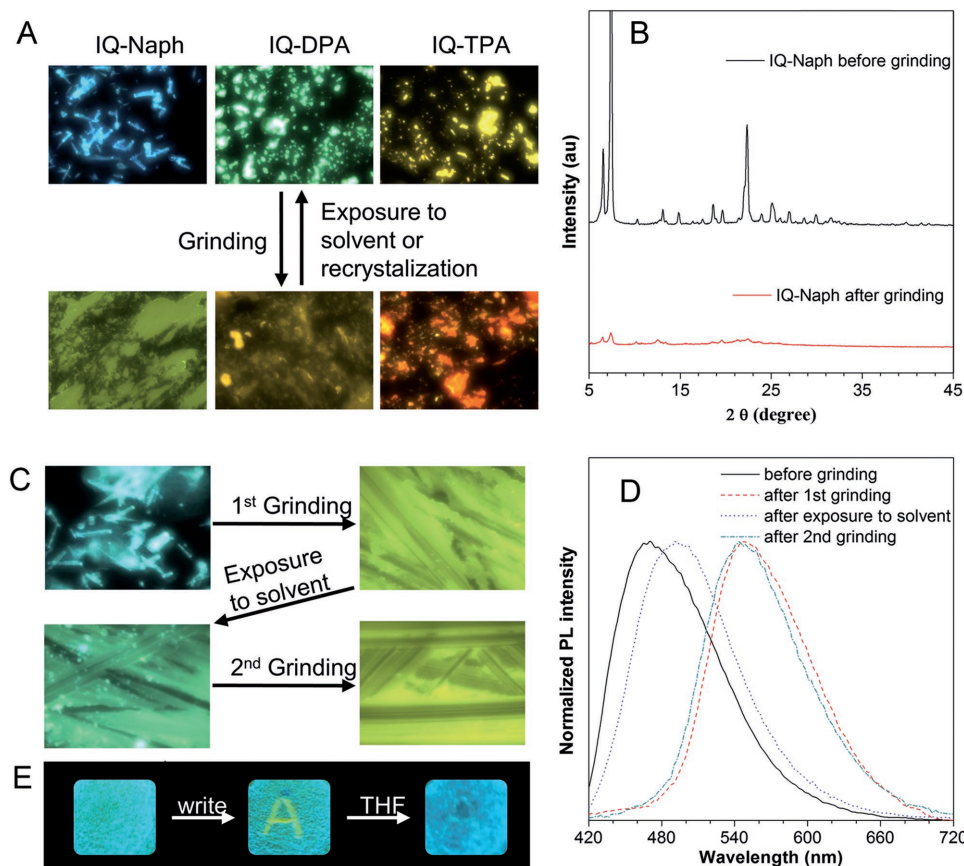


Figure 4. Mechanochromism of IQ-Naph, IQ-DPA, and IQ-TPA. A) Fluorescent images of the corresponding powders of IQ-Naph, IQ-DPA, and IQ-TPA before and after grinding. B) Powder XRD analysis of IQ-Naph. C and D) Fluorescent images and PL spectra of switching the solid-state emissions of IQ-Naph with grinding and exposure to solvent. E) Rewritable paper of IQ-Naph microcrystals. The photos were taken under 365 nm UV irradiation.

are rigidified with multiple weak interactions, resulting in relatively higher quantum yield. After grinding, such weak interactions were destroyed to some extent, the peripheral aryl rings of the molecules can undergo rotations or vibration, and thus the emission in the amorphous state is weakened. The bluer emission observed in the crystals may be attributed to the twisted molecular conformation. While in the amorphous state, they adopted a more planar conformation and thus showing a redder emission.^[17]

Besides studying the color change after grinding, the reversible color switching of these mechanochromic compounds was also investigated. Using IQ-Naph as an example, after exposure to dichloromethane or tetrahydrofuran vapor, the yellow emission of grinded IQ-Naph was reverted to blue emission due to the solvent vapor-induced recrystallization process (Figure 4C,D).^[4c] For an application demonstration, a rewritable paper was made by precipitating fine crystals of IQ-Naph on a filter paper (Figure 4E). The as-prepared paper emits blue emission under UV illumination. After writing with a spatula, a character of “A” with yellow emission was appeared on the paper. When a drop of tetrahydrofuran was added, the yellow emission disappeared. The blue emission was recovered after solvent evaporation. This study well demonstrates the great potential of these mechanochromic compounds in practical applications.

2.5. Mitochondrion-Specific Cell Imaging

Inspired by other cationic lipophilic compounds, such as Mitotracker Red (MTR), Mitotracker Green (MTG), and Rhodamine 123 (Chart S1, Supporting Information), we expect these AIEgens with an inherited cationic structure were mitochondrial targeting in cell imaging due to the driven force of a very large membrane potential of ≈ 180 mV across the mitochondrial membrane.^[21] HeLa cells were incubated with IQ-Naph, IQ-DPA, and IQ-TPA for 10 min and observed under a confocal microscope. The reticulum-like mitochondria of HeLa cells was visualized with a high image contrast by both one-photon excitation (Figure 5A–C) and two-photon excitation (Figure 5D,E). The in situ emission maxima in cells were measured to be 540 nm for IQ-Naph, 550 nm for IQ-DPA, and 570 nm for IQ-TPA (Figure S22, Supporting Information), and pseudocolors of green, yellow, and orange were assigned, respectively, for clarification. Compared to other AIE mitochondrial probes which often have a working concentration of 5 or 10×10^{-6} M and incubation time of 30 min,^[6,20,22] a very low concentration of 200 or 400×10^{-9} M was used with a short staining time of 10 min for IQ-Naph, IQ-DPA, and IQ-TPA, suggesting a good cell permeability and high brightness of these AIEgens when binding to the mitochondrial membranes. Such merits will greatly save the material and time in cell imaging.

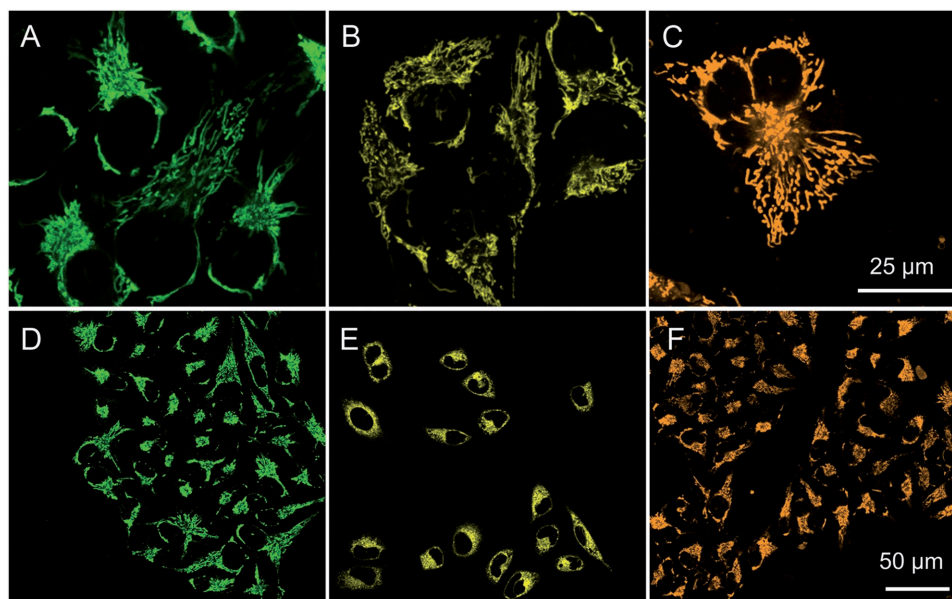


Figure 5. Cell imaging of IQ-Naph, IQ-DPA, and IQ-TPA. A–C) One-photon imaging of HeLa cells stained with A) 200×10^{-9} M IQ-Naph, B) 200×10^{-9} M IQ-DPA, and C) 400×10^{-9} M IQ-TPA for 10 min, respectively. Excitation: 442 nm. Emission: 500–600 nm. Scale bar: 25 μ m. D–F) Two-photon imaging of HeLa cells stained with D) 200×10^{-9} M IQ-Naph, E) 50×10^{-9} M IQ-DPA, and F) 400×10^{-9} M IQ-TPA for 10 min, respectively. Excitation: 820 nm for IQ-Naph, 860 nm for IQ-DPA, and IQ-TPA by Ti:sapphire laser. Emission: 500–600 nm. Scale bar: 50 μ m.

To further confirm the mitochondrial targeting of these AIEgens, the colocalization experiment was performed. MTR with long excitation/emission of 581/644 nm was chosen to avoid overlapping in excitation and emission. As shown in **Figure 6**, the fluorescent images of the fine mitochondrial structures from IQ-Naph, IQ-DPA, and IQ-TPA greatly resemble those from MTR, confirming the specific mitochondrial targeting of these dyes. The Pearson's coefficients were calculated to be 0.7535, 0.8416, and 0.7765 for IQ-Naph, IQ-DPA, and IQ-TPA, respectively. Also, the overlap coefficients were calculated to be 0.7959, 0.8557, and 0.8268 for IQ-Naph, IQ-DPA, and IQ-TPA, respectively. These data suggest the high correlation of the two images and the slight deviation of the coefficients from one were probably due to the slight displacement of the mitochondria caused by the live cell movements between the two frames as indicated by the overlapped images in **Figure 6**.

In addition, biocompatibility and photostability are also two important parameters for cell imaging. The biocompatibility of IQ-Naph, IQ-DPA, and IQ-TPA was assessed by 3-(4,5-dimethyl-2-thiazolyl)-2,5-diphenyltetrazolium bromide (MTT) assays. As the results shown in **Figure 7A**, these AIEgens are biocompatible below 1000×10^{-9} M with almost 80% cell viability after 24 h incubation with HeLa cells. In terms of photostability, almost 100% of fluorescent signals of these AIEgens were retained after 50 scans, while the signal of MTR decreased to 25% within 10 scans (**Figure 7B**), indicating a superior photostability of these AIEgens. Moreover, when the staining concentration was increased, the fluorescence intensity of the stained cells increased all the way with a low background (**Figure S23**, Supporting Information). This should be attributed to RIM and turn-on sensing feature of AIEgens when bind to the mitochondrial membrane. All the results suggest that IQ-Naph, IQ-DPA,

and IQ-TPA are a series of superior mitochondrion-specific probes.

2.6. Cancer Cell-Targeting

To examine MMP-dependent accumulation of these AIEgens, IQ-DPA was chosen as an example to investigate. Prior to the staining process, HeLa cells were treated with membrane-potential stimulants, carbonyl cyanide 3-chlorophenylhydrazone (CCCP) and oligomycin, to decrease or increase MMP, respectively.^[22] Compared to the control experiment, IQ-DPA can no longer effectively accumulate in the mitochondria of cells treated with CCCP, resulting in a decrease in the fluorescence intensity (**Figure 8A**). On the other hand, an enhancement of the fluorescence intensity was observed for cells treated with oligomycin (**Figure 8B**). These results prove that the accumulation or targeting property of IQ-DPA in the mitochondria is strongly dependent on the MMP. Meanwhile, Rhodamine 123, a commercial fluorescent probe to evaluate the mitochondrial membrane potential based on ACQ effect, was used to validate the drug effect. With the increased MMP, the intensity of Rhodamine 123 decreased as more dyes were driven into mitochondria leading to self-quenching. Whereas the fluorescent intensity of Rhodamine 123 increased by decreasing MMP. For qualitative analysis, the ACQ probes is disadvantageous as misinterpretation of the result may occur due to the nonmonotonic relationship between concentration and fluorescence intensity. Oppositely, fluorescence intensity of IQ-DPA can directly represent MMP with a positive monotonic correlation between the fluorescence intensity and the local dye concentration in mitochondria and thus is highly beneficial for MMP analysis.

As MMP-dependent mitochondrial probes, these dyes are potentially applicable in tracking mitochondria for apoptosis

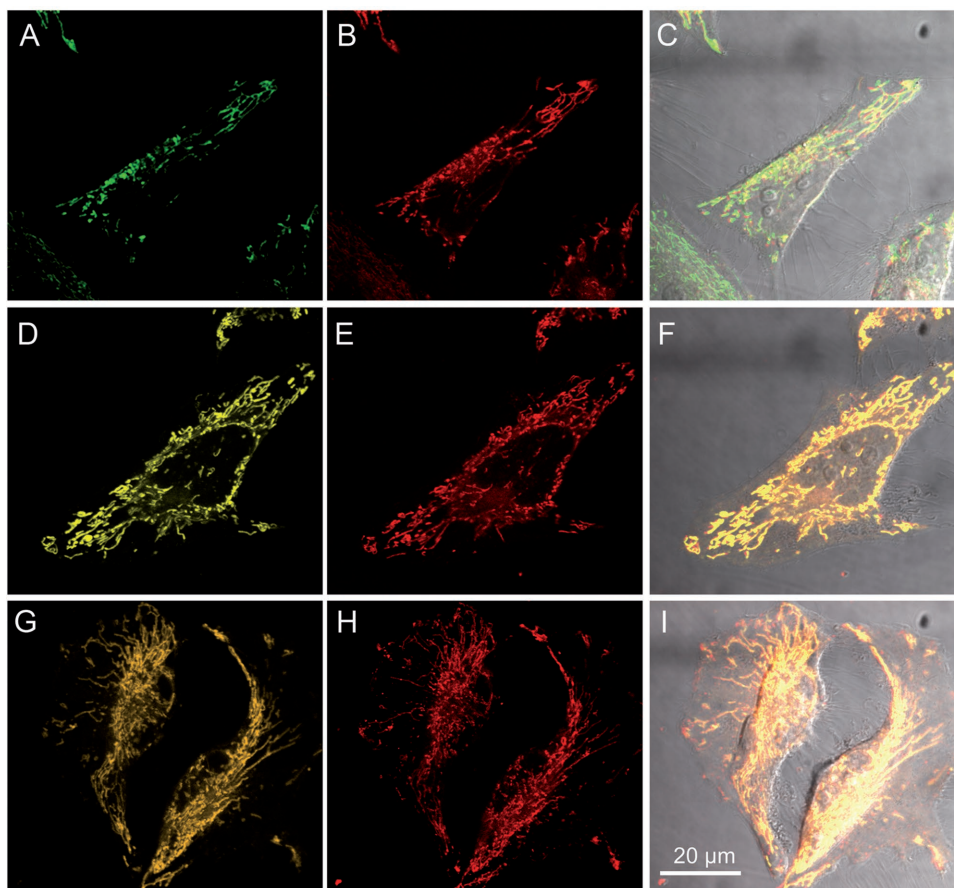


Figure 6. Colocalization of IQ-Naph, IQ-DPA, and IQ-TPA with Mitotracker Red FM. HeLa cells were costained with A–C) IQ-Naph, D–F) IQ-DPA, or G–I) IQ-TPA and 100×10^{-9} M Mitotracker Red FM (MTR) for 15 min. Excitation: 442 nm for IQ-Naph, IQ-DPA, and IQ-TPA and 561 nm for MTR. Emission: 500–600 nm for IQ-Naph, IQ-DPA, and IQ-TPA and 600–700 nm for MTR. Scale bar: 25 μ m.

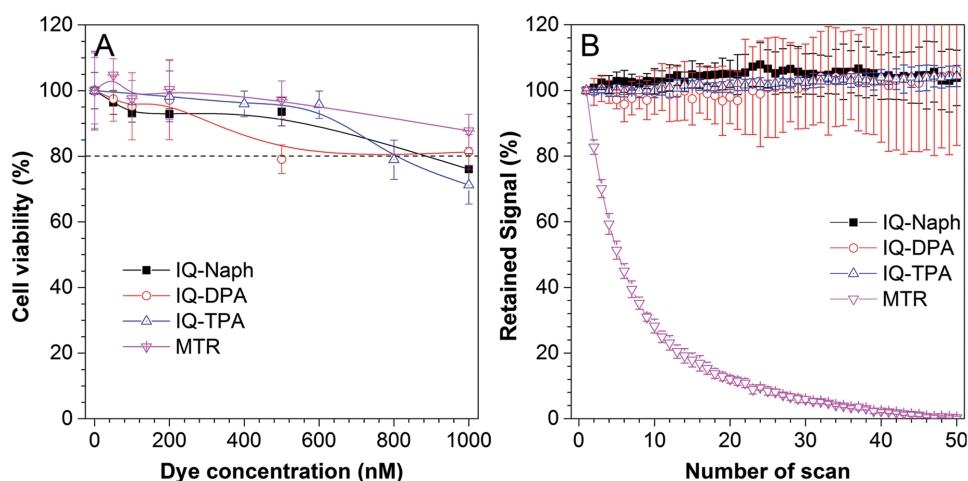


Figure 7. Biocompatibility and photostability. A) Cell viability tested by MTT assays: HeLa cells were incubated with different concentrations of IQ-Naph, IQ-DPA, and IQ-TPA in culture medium for 24 h. B) Photostability: plots of retained signal of IQ-Naph, IQ-DPA, and IQ-TPA or MTR in HeLa cells versus the number of scan. HeLa cells were stained with IQ-Naph (200×10^{-9} M), IQ-DPA (50×10^{-9} M), and IQ-TPA (400×10^{-9} M) or MTR (200×10^{-9} M) in PBS for 10 min, respectively. Excitation: 442 nm for IQ-Naph, IQ-DPA, and IQ-TPA and 561 nm for MTR. Emission: 500–600 nm for IQ-Naph, IQ-DPA, and IQ-TPA and 600–700 nm for MTR. Scanning speed: 5.24 s per scan.

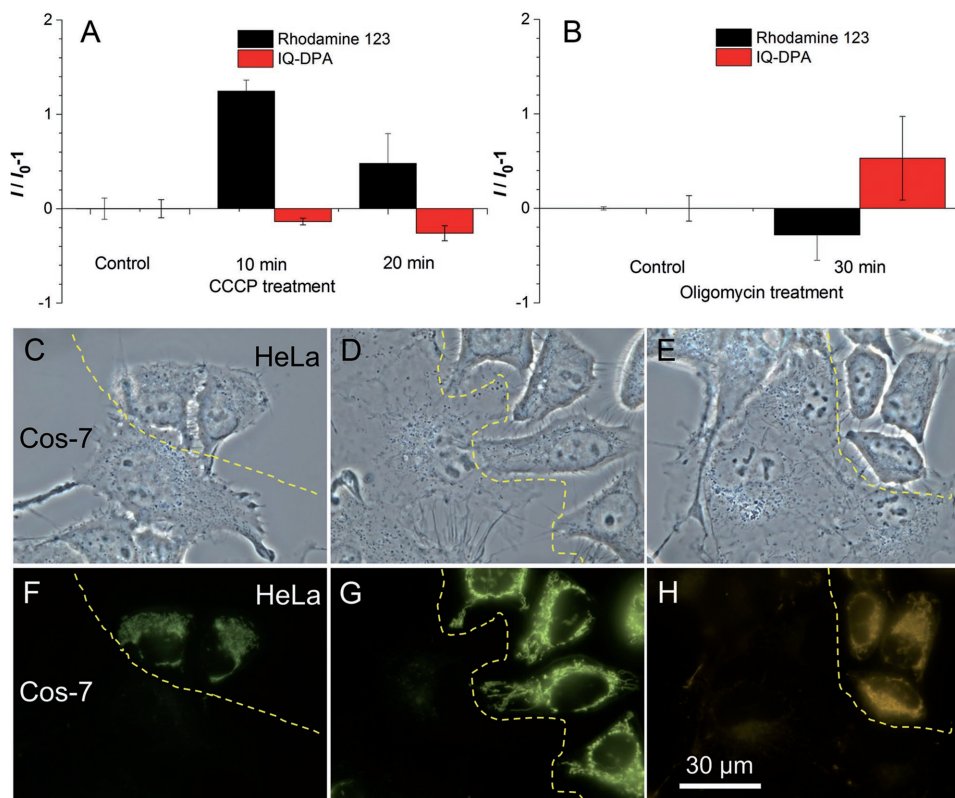


Figure 8. Mitochondrial membrane potential-dependent cellular uptake and cancer cell-targeting. A and B) Fluorescence intensity of HeLa cell pre-treated with A) 50×10^{-6} M CCCP or B) or $10 \mu\text{g mL}^{-1}$ oligomycin in PBS for certain time and then stained with rhodamine 123 (2×10^{-6} M) or IQ-DPA (200×10^{-9} M) for 10 min. C–H) Bright field and fluorescence images of HeLa cells and Cos-7 cells stained by C and F) 200×10^{-9} M IQ-Naph, D and G) 200×10^{-9} M IQ-DPA, and E and H) 400×10^{-9} M IQ-TPA. Excitation wavelength: 400–440 nm for IQ-Naph and IQ-DPA and 460–490 nm for IQ-TPA. Scale bar: 30 μm .

studies,^[23] identifying the differentiating brown adipose cells,^[24] and evaluating sperm activity.^[22] Moreover, it has been reported recently that most cancer cell lines exhibit a much higher MMP than normal cancer lines. Therefore, differentiating cell lines based on MMP would be potentially an approach for imaging-guided cancer ablation.^[25] As a state of the art, HeLa cells with high MMP and Cos-7 with low MMP were coseeded on same glass slide and incubated with the AIE probes. As shown in **Figure 9C–H**, HeLa cells appear much more emissive than Cos-7 cells, indicating the great potential of these dyes for imaging-guided cancer ablation.

2.7. Bacterial Imaging

With the good cell imaging performance, we further explored our synthesized AIEgens in bacterial imaging by using *E. coli* as a model. Due to the fluorescence “turn-on” characteristics upon binding, AIE probes can be used with a wash-free fashion in bacterial imaging, which are of significance for health care, food processing, and medical hygiene.^[26] After incubation with IQ-Naph, IQ-DPA, and IQ-TPA at the concentration of 2×10^{-6} M for 10 min, clearly, hollow fluorescent images of *E. coli* bacteria were observed (Figure 9A), indicating these AIEgens can bind to the surface of the *E. coli*. With positive charges, these AIEgens are expected to bind onto the bacteria

based on the electrostatic and hydrophobic interactions and the high fluorescence intensity should be attributed to the RIM induced by the trap of dyes in the bacterial walls or membrane.^[27] Since these AIEgens are well dissolved in the PBS at the working concentration and almost nonemissive, there is no need of wash-step after staining, which will greatly relieve the workload of bacterial staining. Moreover, costaining with propidium iodide (PI) was performed. As PI can selectively stain the dead bacteria with strong red fluorescence, the results in Figure 9B reveal that both live and dead bacteria can be stained by these AIEgens. Then, *E. coli* viabilities after 24 h incubation of these AIEgens were evaluated to be over 80% by plate counting method (Figure S24, Supporting Information), indicating a good biocompatibility of these AIEgens toward *E. coli*.

3. Conclusion

In conclusion, a facile one-pot synthesis was applied to develop three new double bond-free AIEgens, IQ-Naph, IQ-DPA, and IQ-TPA, with high stability and multifunctionalities. By attachment of different electron donor groups to the electron-deficient isoquinolinium core, their emission colors can be readily tuned with both visible one-photon and susceptible near-infrared two-photon excitations. Theoretical optimizations and single crystal structures revealed that the rotatable phenyl

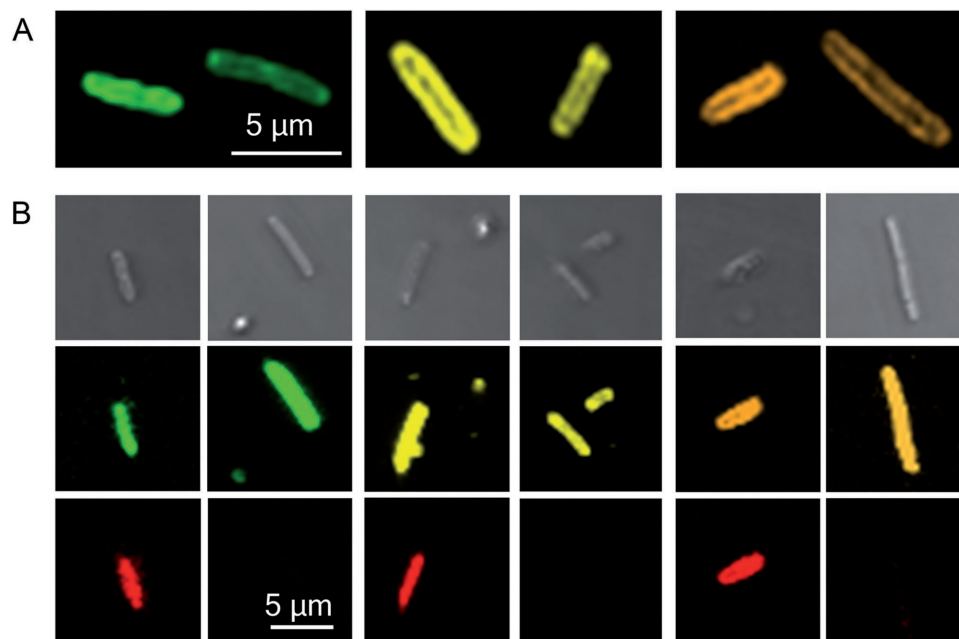


Figure 9. Bacterial imaging of IQ-Naph, IQ-DPA, and IQ-TPA. A) Confocal images of *E. coli* stained by IQ-Naph, IQ-DPA, and IQ-TPA excited at 840 nm, respectively. B) Bright fields (row 1) and confocal images (row 2) of *E. coli* stained by IQ-Naph, IQ-DPA, or IQ-TPA, respectively, and costained with 1.5×10^{-6} M PI (row 3, red color). Excitation: 442 nm for IQ-Naph, IQ-DPA, and IQ-TPA and 561 nm for PI. Emission: 500–600 nm for IQ-Naph, IQ-DPA, and IQ-TPA, and 600–700 nm for PI. Dye concentration: 2×10^{-6} M. Scale bar: 5 μ m.

groups together with twisted conformations are responsible for the AIE features of these compounds. In terms of practical applications, these AIEgens exhibit mechanochromism with large emission shift of up to 78 nm and can be applied for rewritable papers with high contrast. Also, they can serve as superior mitochondrial probes with excellent cell permeability, high brightness, good biocompatibility, and excellent photostability. The short staining time and low working concentration are beneficial to largely save the materials and experimental time. Their MMP-dependent cellular uptake is promising for application in evaluation of MMP and image-guided cancer cell ablation. Moreover, they are useful turn-on imaging probes for bacterial with a wash-free manner, which will greatly relieve the workload of bacterial staining. All these intriguing results suggest the diphenyl isoquinolinium-based AIEgens built by the one-pot method would provide a new platform of AIEgens for various high-tech applications.

4. Experimental Section

Materials, instrumentation, and detailed experimental procedures can be found in the Supporting Information.

CCDC 1561007 and 1561006 contain the supplementary crystallographic data for this paper. These data can be obtained free of charge from The Cambridge Crystallographic Data Centre via www.ccdc.cam.ac.uk/data_request/cif.

Supporting Information

Supporting Information is available from the Wiley Online Library or from the author.

Acknowledgements

This work was partially supported by the National Basic Research Program of China (973 Program: 2013CB834701 and 2013CB834702), the University Grants Committee of Hong Kong (AoE/P-03/08 and AoE/P-02/12), the Research Grants Council of Hong Kong (16301614, 16305015, 16308016, N-HKUST604/14, and A-HKUST605/16), and the Innovation and Technology Commission (ITC-CNERC14SC01 and ITCPD/17-9). B.Z.T. is also grateful for the support from the Guangdong Innovative Research Team Program of China (201101C0105067115), the Science and Technology Plan of Shenzhen (JCYJ20160229205601482), and the Shenzhen Peacock Plan.

Conflict of Interest

The authors declare no conflict of interest.

Keywords

aggregation-induced emission, bacterial imaging, mechanochromism, mitochondrial imaging, multifunctionality

Received: August 11, 2017
Revised: September 10, 2017
Published online: November 9, 2017

- [1] a) H. Kobayashi, M. Ogawa, R. Alford, P. L. Choyke, Y. Urano, *Chem. Rev.* **2010**, *110*, 2620; b) R. W. Sinkeldam, N. J. Greco, Y. Tor, *Chem. Rev.* **2010**, *110*, 2579; c) J. Wu, W. Liu, J. Ge, H. Zhang, P. Wang, *Chem. Soc. Rev.* **2011**, *40*, 3483.
[2] a) J. Mei, N. L. C. Leung, R. T. K. Kwok, J. W. Y. Lam, B. Z. Tang, *Chem. Rev.* **2015**, *115*, 11718; b) N. L. C. Leung, N. Xie, W. Yuan,

- Y. Liu, Q. Wu, Q. Peng, Q. Miao, J. W. Y. Lam, B. Z. Tang, *Chem. - Eur. J.* **2014**, *20*, 15349; c) S. Kumar, P. Singh, A. Mahajan, S. Kumar, *Org. Lett.* **2013**, *15*, 3400; d) C.-X. Yuan, X.-T. Tao, Y. Ren, Y. Li, J.-X. Yang, W.-T. Yu, L. Wang, M.-H. Jiang, *J. Phys. Chem. C* **2007**, *111*, 12811.
- [3] a) J. Luo, Z. Xie, J. W. Y. Lam, L. Cheng, B. Z. Tang, H. Chen, C. Qiu, H. S. Kwok, X. Zhan, Y. Liu, D. Zhu, *Chem. Commun.* **2001**, 1740; b) L. Yan, Y. Zhang, B. Xu, W. Tian, *Nanoscale* **2016**, *8*, 2471; c) Y. Hong, *Methods Appl. Fluoresc.* **2016**, *4*, 022003.
- [4] a) R. Misra, T. Jadhav, B. Dhokale, S. M. Mobin, *Chem. Commun.* **2014**, *50*, 9076; b) C. Y. Y. Yu, R. T. K. Kwok, J. Mei, Y. Hong, S. Chen, J. W. Y. Lama, B. Z. Tang, *Chem. Commun.* **2014**, *50*, 8134; c) T. Hu, B. Yao, X. Chen, W. Li, Z. Song, A. Qin, J. Z. Sun, B. Z. Tang, *Chem. Commun.* **2015**, *51*, 8849; d) Y. Zhao, C. Y. Y. Yu, R. T. K. Kwok, Y. Chen, S. Chen, J. W. Y. Lam, B. Z. Tang, *J. Mater. Chem. B* **2015**, *3*, 4993.
- [5] a) J. He, B. Xu, F. Chen, H. Xia, K. Li, L. Ye, W. Tian, *J. Phys. Chem. C* **2009**, *113*, 9892; b) N. Song, D.-X. Chen, M.-C. Xia, X.-L. Qiu, K. Ma, B. Xu, W. Tian, Y.-W. Yang, *Chem. Commun.* **2015**, *51*, 5526.
- [6] Z. Song, W. Zhang, M. Jiang, H. H. Y. Sung, R. T. K. Kwok, H. Nie, I. D. Williams, B. Liu, B. Z. Tang, *Adv. Funct. Mater.* **2016**, *26*, 824.
- [7] J. Chen, B. Xu, X. Ouyang, B. Z. Tang, Y. Cao, *J. Phys. Chem. A* **2004**, *108*, 7522.
- [8] a) W. Tang, Y. Xiang, A. Tong, *J. Org. Chem.* **2009**, *74*, 2163; b) M. Yang, D. Xu, W. Xi, L. Wang, J. Zheng, J. Huang, J. Zhang, H. Zhou, J. Wu, Y. Tian, *J. Org. Chem.* **2013**, *78*, 10344.
- [9] a) A. Singh, C.-K. Lim, Y.-D. Lee, J.-H. Maeng, S. Lee, J. Koh, S. Kim, *ACS Appl. Mater. Interfaces* **2013**, *5*, 8881; b) X. Zhao, P. Xue, K. Wang, P. Chen, P. Zhang, R. Lu, *New J. Chem.* **2014**, *38*, 1045.
- [10] a) J. Mei, J. Wang, J. Z. Sun, H. Zhao, W. Yuan, C. Deng, S. Chen, H. H. Sung, P. Lu, A. Qin, *Chem. Sci.* **2012**, *3*, 549; b) L. Chen, Y. Jiang, H. Nie, P. Lu, H. H. Y. Sung, I. D. Williams, H. S. Kwok, F. Huang, A. Qin, Z. Zhao, B. Z. Tang, *Adv. Funct. Mater.* **2014**, *24*, 3621; c) B. Chen, G. Feng, B. He, C. Goh, S. Xu, G. Ramos-Ortiz, L. Aparicio-Ixta, J. Zhou, L. Ng, Z. Zhao, B. Liu, B. Z. Tang, *Small* **2016**, *12*, 782.
- [11] a) Y. Yang, X. Su, C. N. Carroll, I. Aprahamian, *Chem. Sci.* **2012**, *3*, 610; b) D. Zhao, G. Li, D. Wu, X. Qin, P. Neuhaus, Y. Cheng, S. Yang, Z. Lu, X. Pu, C. Long, J. You, *Angew. Chem., Int. Ed.* **2013**, *52*, 13676; c) K. Tanaka, Y. Chujo, *NPG Asia Mater.* **2015**, *7*, e223.
- [12] M. Chen, L. Li, H. Nie, J. Tong, L. Yan, B. Xu, J. Z. Sun, W. Tian, Z. Zhao, A. Qin, B. Z. Tang, *Chem. Sci.* **2015**, *6*, 1932.
- [13] a) J. Wang, J. Mei, R. Hu, J. Z. Sun, A. Qin, B. Z. Tang, *J. Am. Chem. Soc.* **2012**, *134*, 9956; b) K. Garg, E. Ganapathi, P. Rajakannu, M. Ravikanth, *Phys. Chem. Chem. Phys.* **2015**, *17*, 19465; c) X. Guo, J. Zhou, M. A. Siegler, A. E. Bragg, H. E. Katz, *Angew. Chem., Int. Ed.* **2015**, *54*, 4782; d) T. T. Tasso, T. Furuyama, N. Kobayashi, *Chem.-Eur. J.* **2015**, *21*, 4817.
- [14] a) S. Chen, Y. Hong, Y. Liu, J. Liu, C. W. Leung, M. Li, R. T. Kwok, E. Zhao, J. W. Lam, Y. Yu, *J. Am. Chem. Soc.* **2013**, *135*, 4926; b) S. Chen, Y. Hong, J. Liu, N.-W. Tseng, Y. Liu, E. Zhao, J. W. Yip Lam, B. Z. Tang, *J. Mater. Chem. B* **2014**, *2*, 3919; c) Y. Zhang, D. Li, Y. Li, J. Yu, *Chem. Sci.* **2014**, *5*, 2710; d) W. Chen, Z. Zhang, X. Li, H. Agren, J. Su, *RSC Adv.* **2015**, *5*, 12191; e) J. Tong, Y. Wang, J. Mei, J. Wang, A. Qin, J. Z. Sun, B. Z. Tang, *Chem. - Eur. J.* **2014**, *20*, 4661.
- [15] a) K. Parthasarathy, N. Senthilkumar, J. Jayakumar, C.-H. Cheng, *Org. Lett.* **2012**, *14*, 3478; b) J. Jayakumar, K. Parthasarathy, C.-H. Cheng, *Angew. Chem., Int. Ed.* **2012**, *51*, 197; c) E. Zhao, H. Deng, S. Chen, Y. Hong, C. W. T. Leung, J. W. Y. Lam, B. Z. Tang, *Chem. Commun.* **2014**, *50*, 14451; d) N. Senthilkumar, P. Gandeepan, J. Jayakumar, C.-H. Cheng, *Chem. Commun.* **2014**, *50*, 3106.
- [16] N. Zhao, Z. Yang, J. W. Y. Lam, H. H. Y. Sung, N. Xie, S. Chen, H. Su, M. Gao, I. D. Williams, K. S. Wong, B. Z. Tang, *Chem. Commun.* **2012**, *48*, 8637.
- [17] Y. Q. Dong, J. W. Y. Lam, B. Z. Tang, *J. Phys. Chem. Lett.* **2015**, 3429.
- [18] a) H. Zhang, J. Fan, H. Dong, S. Zhang, W. Xu, J. Wang, P. Gao, X. Peng, *J. Mater. Chem. B* **2013**, *1*, 5450; b) Z. Zhao, B. Chen, J. Geng, Z. Chang, L. Aparicio-Ixta, H. Nie, C. C. Goh, L. G. Ng, A. Qin, G. Ramos-Ortiz, B. Liu, B. Z. Tang, *Part. Part. Syst. Charact.* **2014**, *31*, 481; c) J. Y. Koo, C. H. Heo, Y.-H. Shin, D. Kim, C. S. Lim, B. R. Cho, H. M. Kim, S. B. Park, *Chem. - Eur. J.* **2016**, *22*, 14166; d) M. Jiang, X. Gu, J. W. Y. Lam, Y. Zhang, R. T. K. Kwok, K. S. Wong, B. Z. Tang, *Chem. Sci.* **2017**, *8*, 5440; e) Y. Zhang, M. Jiang, G.-C. Han, K. Zhao, B. Z. Tang, K. S. Wong, *J. Phys. Chem. C* **2015**, *119*, 27630; f) H. M. Kim, B. R. Cho, *Chem. Rev.* **2015**, *115*, 5014.
- [19] a) S. Mo, Q. Meng, S. Wan, Z. Su, H. Yan, B. Z. Tang, M. Yin, *Adv. Funct. Mater.* **2017**, *27*, 1701210; b) P. Ganesan, R. Ranganathan, Y. Chi, X.-K. Liu, C.-S. Lee, S.-H. Liu, G.-H. Lee, T.-C. Lin, Y.-T. Chen, P.-T. Chou, *Chem. - Eur. J.* **2017**, *23*, 2858.
- [20] N. Zhao, M. Li, Y. Yan, J. W. Lam, Y. L. Zhang, Y. S. Zhao, K. S. Wong, B. Z. Tang, *J. Mater. Chem. C* **2013**, *1*, 4640.
- [21] a) S. Davis, M. J. Weiss, J. R. Wong, T. J. Lampidis, L. B. Chen, *J. Biol. Chem.* **1985**, *260*, 13844; b) L. B. Chen, *Annu. Rev. Cell Biol.* **1988**, *4*, 155; c) C. W. T. Leung, Y. Hong, S. Chen, E. Zhao, J. W. Y. Lam, B. Z. Tang, *J. Am. Chem. Soc.* **2013**, *135*, 62.
- [22] N. Zhao, S. Chen, Y. Hong, B. Z. Tang, *Chem. Commun.* **2015**, *51*, 13599.
- [23] J. D. Ly, D. R. Grubb, A. Lawen, *Apoptosis* **2003**, *8*, 115.
- [24] M. Gao, C. K. Sim, C. W. T. Leung, Q. Hu, G. Feng, F. Xu, B. Z. Tang, B. Liu, *Chem. Commun.* **2014**, *50*, 8312.
- [25] a) L. Zhang, W. Liu, X. Huang, G. Zhang, X. Wang, Z. Wang, D. Zhang, X. Jiang, *Analyst* **2015**, *140*, 5849; b) C.-J. Zhang, Q. Hu, G. Feng, R. Zhang, Y. Yuan, X. Lu, B. Liu, *Chem. Sci.* **2015**, *6*, 4580; c) C. Gui, E. G. Zhao, R. T. K. Kwok, A. C. S. Leung, J. W. Y. Lam, M. J. Jiang, H. Q. Deng, Y. J. Cai, W. J. Zhang, H. F. Su, B. Z. Tang, *Chem. Sci.* **2017**, *8*, 1822.
- [26] a) E. Zhao, Y. Hong, S. Chen, C. W. T. Leung, C. Y. K. Chan, R. T. K. Kwok, J. W. Y. Lam, B. Z. Tang, *Adv. Healthcare Mater.* **2014**, *3*, 88; b) M. Gao, Q. Hu, G. Feng, N. Tomczak, R. Liu, B. Xing, B. Z. Tang, B. Liu, *Adv. Healthcare Mater.* **2015**, *4*, 659; c) E. Zhao, Y. Chen, S. Chen, H. Deng, C. Gui, C. W. Leung, Y. Hong, J. W. Lam, B. Z. Tang, *Adv. Mater.* **2015**, *27*, 4931; d) E. Zhao, Y. Chen, H. Wang, S. Chen, J. W. Y. Lam, C. W. T. Leung, Y. Hong, B. Z. Tang, *ACS Appl. Mater. Interfaces* **2015**, *7*, 7180.
- [27] G. Jiang, J. Wang, Y. Yang, G. Zhang, Y. Liu, H. Lin, G. Zhang, Y. Li, X. Fan, *Biosens. Bioelectron.* **2016**, *85*, 62.